Development of a Damageable Numerical Engine Cooling System for Resilient Aerospike Rockets

Marco Nanni[1], Seungho Rhee[2], James Canino[3]
Ray W. Herrick Laboratories, School of Aeronautics and Astronautics, Purdue University, West Lafayette, IN, 47907-2099

Federico Rossi[4], Ernesto Sozio[5]
Pangea Aerospace, Barcelona, Spain

and

Davide Ziviani[6]
Ray W. Herrick Laboratories, School of Mechanical Engineering, Purdue University, West Lafayette, IN, 47907-2099

The role of a resilient aerospike rocket engine system, including both propulsion and thermal management systems, is to ensure mission success during nominal and emergency operations for long-term space explorations. Abnormal flight conditions can drastically impact component performance, leading to cascading damage effects across the entire system. While existing research has optimized regenerative cooling systems for rocket engines under steady-state, or during normal engine operations, a critical gap remains in analyzing system-level interactions with damaged components. To address this gap, this paper introduces a multi-physics system-level numerical model of the thermal management system of the aerospike rocket. First, a literature review of the state-of-the-art in aerospike engines is conducted to identify baseline requirements and establish the design operating conditions. Subsequently, the system behaviors are evaluated using the introduced model to investigate the impact of degraded components on the performance of the aerospike combustion chamber and the nozzle's cooling system. This paper provides a baseline for further studies aimed at enhancing the robustness and resilience of the aerospike's thermal management system.

Acronyms and Nomenclature

A	= Surface area, m^2	$\dot{q}$	= Heat flux, W/m^2
c_{eff}^*	= Characteristic exhaust velocity efficiency	$\dot{Q}$	= Heat transfer rate, W
Cp	= Specific heat at const. pressure, $kJ/(kg \cdot K)$	R	= Universal gas constant, $J/(mol \cdot K)$
F	= Thrust, N	Re	= Reynolds number
$GGMRCV$	= Gas Generator Mixture Ratio Control Valve	t	= Time, s
h	= Specific enthalpy, J/kg	T	= Temperature, K
HTC	= Convection heat transfer coefficient, $W/(m^2 \cdot K)$	TCV	= Thrust Control Valve
J	= Moment of inertia, $kg \cdot m^2$	TMS	= Thermal Management System
K	= Flow coefficient, $kg^{1/2} \cdot m^{1/2}$	Trq	= Torque, $N \cdot m$
k	= Thermal conductivity, $W/(m \cdot K)$	v	= Velocity, m/s
LOX	= Liquid oxygen	Vol	= Volume, m^3
LCF	= Low cycle fatigue	$\dot{W}$	= Power, W

[1] M.S. student, School of Aeronautics and Astronautics, West Lafayette, IN, 47907-2099.

[2] Ph.D. Student, School of Mechanical Engineering, West Lafayette, IN, 47907-2099.

[3] Asso. Professor of Engineering Practice, School of Aeronautics and Astronautics, West Lafayette, IN, 47907-2099.

[4] Head of Propulsion Engineering, Barcelona, Spain.

[5] Senior Propulsion Aerodynamics Engineer, Barcelona, Spain.

[6] Associate Professor, School of Mechanical Engineering, West Lafayette, IN, 47907-2099

$MRCV$	= Mixture Ratio Control Valve	Pr	= Prandtl number
$\dot{m}$	= Mass flow rate, kg/s	α	= Thermal diffusivity, m^2/s
MW	= Molecular weight, $kg/kmol$	β	= Pump blade deflection angle
N_{rad}	= Angular velocity of pump shaft, rad/s	γ	= Specific heat ratio
Nu	= Nusselt number	η	= Efficiency
$NPSH$	= Net Positive Suction Head, m	ρ	= Density, kg/m^3
O/F	= Oxidizer-to-fuel ratio	μ	= Dynamic viscosity, $Pa \cdot s$
P	= Pressure, Pa		

Subscript

cc	= Combustion chamber	th	= Nozzle throat
o	= Oxidizer	m,out	= Meridional at impeller outlet
f	= Fuel	t,out	= Tangential at impeller outlet
gg	= Gas generator	e	= Exit
t	= Turbine	vol	= Volumetric
p	= Pump	$mech$	= Mechanical
l	= Coolant	gas	= Gas in combustion chamber/nozzle

I. Introduction

AEROSPIKE engines offer superior propellant efficiency in both atmospheric and vacuum conditions, making them ideal for planetary and interplanetary missions[1]. However, these benefits come with higher thermal loads during normal operations[2,3,4]. Russo Sorge et al.[2] identified the highest heat flux at the nozzle throat, necessitating an effective cooling system. Significant efforts have been made to optimize cooling channel geometry for enhanced heat transfer. Pizzarelli et al.[5] showed that increasing aspect ratio improves cooling up to AR=10, beyond which diminishing returns and manufacturing complexity arise due to thermal stratification. Mullin et al.[6] demonstrated that increasing turbulent mixing enhances cooling performance.

Jeon et al.[7] analyzed coolant exit conditions on system performance but only under steady-state assumptions, ignoring transient or off-nominal conditions. While these studies improve thermal management system efficiency, they primarily focus on optimizing reliability and performance under steady-state and transient conditions. However, resilience, the ability of a system to adapt and maintain function despite unexpected failures[7], requires assessing system-level interactions and the effects of component degradation on the cooling system.

Given the importance of resilience and the gaps in prior research, this paper introduces a multi-physics system-level model to assess how damaged components impact the aerospike engine's thermal management system, during a time-dependent simulation representing a typical mission profile. This model will serve as a foundational step to enable the design of future resilient aerospike engines.

II. Aerospike Thermal Management System Overview

The thermal management system in the aerospike is fundamental to ensure that the engine will operate within certain limit temperatures, and thus maintain structural integrity. In fact, a rocket combustion chamber can develop heat fluxes higher than 8 kilowatt per cubic meter [8], which requires an appropriate cooling system to maintain the wall between coolant and hot gases below allowable limits.

On the right side of Figure 1 a typical aerospike rocket engine with 24 combustion chambers/nozzles arranged around an external plug, or spike, is illustrated. Propellant is injected into these combustion chambers/nozzles, where it reacts and partially expands before being ejected onto the external plug contour. Here, it expands further, reaching atmospheric pressure[1]. The left side of Figure 1 provides a schematic representation of the engine system, illustrating one of the 24 combustion chambers/nozzles and one side of the plug contour below it. As shown in Figure 1, the thermal management of the designed rocket system utilizes both the fuel and oxidizer in a gas-generator cycle configuration. Therefore, the entire flow path of the fuel and oxidizer must be simulated to properly evaluate the thermal management of the rocket. The flow path starts with the propellant tanks and pumps, which set enough pressure to drive the propellant through the regenerative cooling channels (or cooling jacket) and into the manifold
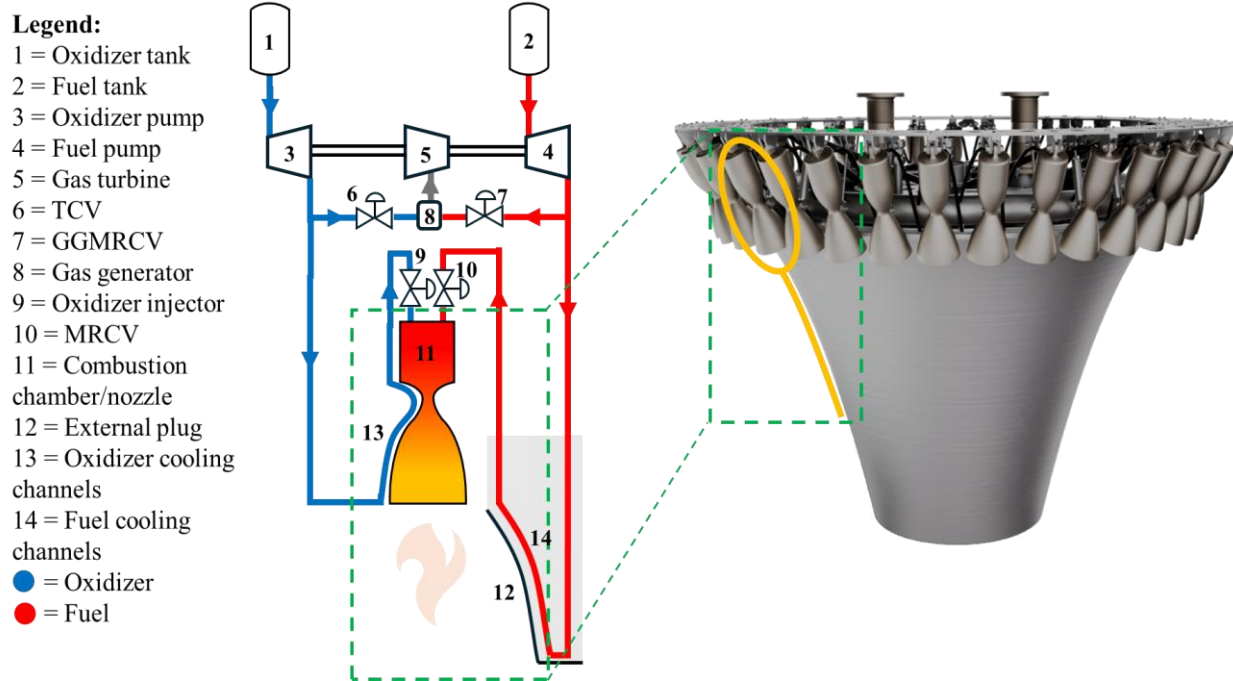
Legend:
1 = Oxidizer tank
2 = Fuel tank
3 = Oxidizer pump
4 = Fuel pump
5 = Gas turbine
6 = TCV
7 = GGMRCV
8 = Gas generator
9 = Oxidizer injector
10 = MRCV
11 = Combustion chamber/nozzle
12 = External plug
13 = Oxidizer cooling channels
14 = Fuel cooling channels
● = Oxidizer
● = Fuel

Figure 1. On the left: Aerospike engine (courtesy of Pangea Aerospace[23]). On the right: Zoomed-in view of a combustion chamber/nozzle element and plug from the Aerospike engine on the left.

before the injectors. The system includes multiple heat exchangers for the 24 oxygen-cooled combustion chambers/nozzles and the methane-cooled external spike. Control valves (TCV, MRCV and GGMRCV) are used to simulate throttling performance and the injectors are modeled to determine the impact of changes in flow rate on the properties inside of the combustion chamber. The thrust of the engine is determined after the propellants are injected into the combustion chamber.

   In a gas-generator cycle, the pumps are driven by a gas turbine, which is operated by combustion products from the gas generator. The latter is a small combustor where a portion of fuel and oxidizer are burnt to generate the necessary gas to drive the turbine. The next paragraphs include more details about the functioning and the governing equations characterizing each component of the thermal management system.

III.   Development of Thermal Management System Model

   This section provides an in-depth analysis of the functioning and governing equations of each component of the thermal management system, as outlined in Section II.

A. Regenerative cooling system model

   The Regenerative cooling system consists of a series of cooling channels milled into the combustion chamber and aerospike plug. More recently the cooling channels can also be included in the manufacturing of the combustion chambers and aerospace plug when additive manufacturing is used to make these components.[10] Figure 2 shows the functioning of the regenerative cooling system in rocket engines. Here, the cryogenic propellant, before being injected in the combustion chamber, passes through the cooling channels absorbing some of the heat from the hot gas in the nozzle/combustion chamber, ensuring that the solid wall dividing the hot gas from the propellant will remain at an

Figure 2. Regenerative cooling system.

acceptable temperature[11]. The nozzle/combustion chamber modules are oxygen-cooled, while the external plug is cooled with liquid methane. All of them are assumed to be made of GRCop-42, which is a high temperature copper-alloy often used in these applications[12].
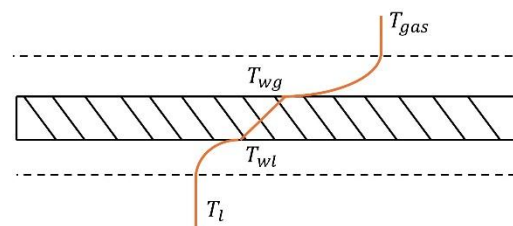
International Conference on Environmental Systems

1. Coolant Governing Equations

The coolant channels are broken up into 190 control volumes along the length of the nozzle or plug. For this study, the coolant dynamic is assumed to be very fast, meaning that the coolant behavior is considered to be quasi-steady for each control volume. This means that conservation of mass, momentum, and energy are considered at steady state for each time step, but the model is still impacted by changes in boundary conditions. This allows the model to predict the new steady-state performance of the cooling channels if, for example, the fuel pump is damaged.

The set of equations are

$$\frac{d\dot{m}}{dt} = 0 \tag{1}$$

$$\Delta P = \frac{1}{2}\rho v^2 f \frac{L}{D} \tag{2}$$

$$\dot{Q} = \dot{m}(h_{out} - h_{in}) \tag{3}$$

where f is the friction factor coefficient found with the Colebrook–White equation:

$$\frac{1}{\sqrt{f}} = -2\,log_{10}\left(\frac{\frac{\epsilon}{D}}{3.7} + \frac{2.51}{Re_l \cdot \sqrt{f}}\right) \tag{4}$$

here ϵ, D are the surface roughness and channel diameter.

2. Solid Wall Governing Equations

As mentioned above, the solid wall is made of GRCop-42, a high temperature material often used for aerospace applications due to its high thermal conductivity and high yield strength at high temperatures[12]. To model the distribution of the wall temperature the conduction differential equation was be used:

$$\frac{\partial T}{\partial t} = \alpha \frac{\partial^2 T}{\partial x^2} \tag{5}$$

To solve the parabolic differential equation the method of lines[13] was used. This equation requires an initial condition and two boundary conditions. The former is taken as the steady state temperature profile during normal engine operations, while the convective heat transfer boundary conditions are used on both sides of the wall. This heat transfer model is used to calculate the temperature change as a function of time and distance within the wall. The convective heat transfer used for the boundary conditions is calculated with the Newton's law of cooling, that is:

$$\dot{Q}_{gas} = HTC_g\, A_{surf}\, (T_r - T_{wg}) \tag{6}$$

$$\dot{Q}_{cool} = HTC_l\, A_{surf}\, (T_{wl} - T_l) \tag{7}$$

where Q is the heat flow, HTC is the convective heat transfer coefficient, and T_r, T_{wg}, T_{wl}, T_l are respectively the recovery temperature of the gas, the temperature of the wall on the hot gas side, the temperature of the wall in the coolant side, and the temperature of the coolant in the channel.

The recovery temperature is often used to model the heat transfer in rocket combustion chambers to account for the compressible boundary layer on rocket nozzles[8], and it is defined as:

$$T_r = T_{gas} \cdot \left(1 + \frac{\gamma - 1}{2} \cdot r \cdot M_{gas}^2\right) \tag{8}$$

where M_{gas} is the gas mach numebr, and r is the recovery factor. For a turbulent boundary layer on a flat plate the recovery factor is given by equation (9) and used to determine the recovery temperature for the combustion gases in this study.

$$r = Pr^{\frac{1}{3}} \tag{9}$$

Given these boundary conditions, the method of lines[16] gives the following expressions for the values that characterize the wall temperature:

$$\frac{dT_{wg}}{dt} = \left(\frac{\alpha}{\Delta x^2}\right)\left(2\,T_{wm} - \left(2\,\Delta x \frac{HTC_g}{k_w} + 2\right)T_{wg} + \left(\Delta x \frac{HTC_g}{k_w}\right)T_r\right) \tag{10}$$

$$\frac{dT_{wm}}{dt} = \left(\frac{\alpha}{\Delta x^2}\right)(T_{wg} - 2\,T_2 + T_{wl}) \tag{11}$$

$$\frac{dT_{wl}}{dt} = \left(\frac{\alpha}{\Delta x^2}\right)\left(2\,T_{wm} - \left(2\,\Delta x \frac{HTC_l}{k_w} + 2\right)T_{wl} + \left(\Delta x \frac{HTC_l}{k_w}\right)T_l\right) \tag{12}$$

where T_{wm} is the temperature in the middle of the wall, Δx is half the wall thickness, α is the thermal diffusivity of the wall, and k_w the wall thermal conductivity.

The heat transfer coefficient for the coolant was calculated using the Gnielinski correlation (Eq. (13)), which is valid over a wide range of Reynolds and Prandtl numbers[16], including those characterizing this case study.

$$Nu = \frac{\left(\frac{f}{8}\right)(Re - 1000)Pr}{1 + 12.7\left(\frac{f}{8}\right)^{0.5}\left(Pr^{\frac{2}{3}} - 1\right)} \tag{13}$$

where Nu is the Nusselt number, k_l, μ_l are the coolant thermal cionductivity and dynamic viscosity, and f is the friction factor, which is found with Equation (4).

For the gas side, the Bartz equation, given in equation (15), is a simple correlation to model the heat transfer coefficient for rocket combustion chambers/nozzles[15].

$$HTC_g = \left(\frac{0.026}{D^{0.2}}\right) \cdot \left(\frac{\mu_{gas_0}^{0.2} \cdot Cp_{gas_0}}{Pr_{gas_0}^{0.6}}\right) \cdot \left(\rho_{gas} \cdot v_{gas}\right)^{0.8} \cdot \left(\frac{T_{gas}}{T_{am}}\right)^{0.8} \cdot \left(\frac{T_{am}}{T_{gas_0}}\right)^{0.2 \cdot w} \tag{15}$$

where $D, \mu_{gas_0}, Cp_{gas_0}, Pr_{gas_0}, \rho_{gas}, Vel_{gas}, T_{gas}, T_{am}, w$, are respectively combustion chamber diameter, gas stagnation viscosity, specific heat, Prandtl number, velocity, temperature, average temperature between recovery temperature T_r and T_{wg}, and w is defined as:

$$w = \frac{log\left(\frac{\mu_{gas}}{\mu_{gas_0}}\right)}{log\left(\frac{T_{gas}}{T_{gas_0}}\right)} \tag{16}$$

As shown in equation (17), the gas side heat transfer coefficient was adjusted using a correction factor of 1/3.

$$HTC_{g_{model}} = \frac{1}{3} \cdot HTC_{g_{Bartz}} \tag{17}$$

This choice assumes that the combustion chambers and nozzles are film-cooled. In this context, film cooling involves injecting liquid fuel along the inner wall of the combustion chamber. This technique reduces heat flux to the solid wall by creating a protective liquid film, which enhances thermal resistance through convective effects. Miranda et al.[17] demonstrated that wall heat flux can decrease significantly with film cooling: from approximately 122 MW/m² without film cooling, to 49 MW/m² using 11 kg/s of liquid H_2 as coolant, and further down to 16 MW/m² with 20 kg/s of H_2. This highlights the strong correlation between increased film mass flow rate and enhanced cooling effectiveness.

B. Turbopumps model

The turbopump assembly consists of an oxygen pump, a fuel pump, and a gas turbine, with a single shaft connecting the components. A gearing system is used so that each pump can operate at a different shaft rotational speed.

1. Pump Governing Equations

The pump was designed based on the specified values for pressure rise, mass flow rate, and NPSH. These values were used to determine the pump's geometric parameters, such as the inlet and outlet radius, vane width, volute, and deflection angle. Additionally, the design rotational speed was also determined[11]. With these design parameters known, the following equations were used to find pump head rise, power consumption, and torque as a function of mass flow rate and rotational speed.

$$U_{out} = N_{rad_p} \cdot r_{out} \tag{18}$$

$$c_{m,out} = \frac{\left(\frac{\dot{m}}{\rho_{in}}\right)}{(2 \cdot \pi \cdot r_{out} \cdot b_{out})} \tag{19}$$

$$c_{t,out} = U_{out} - \frac{c_{m,out}}{tan(\beta_{out})} \tag{20}$$

$$\Delta P_p = (\rho_{in} \cdot \eta_p) \cdot (U_{out} \cdot c_{t,out}) \tag{21}$$

$$P_{out} = P_{in} + \Delta P_p \tag{22}$$

$$\Delta Head = \frac{P_{out} - P_{in}}{g \cdot \rho_{in}} \tag{23}$$

$$\dot{W}_p = \frac{\dot{m} \cdot g \cdot \Delta Head}{\eta_p} \tag{24}$$

$$Trq_p = \frac{\dot{W}_p}{N_{rad_p}} \tag{25}$$

The subscript out stands for the outlet condition of the pump, since the inlet is assumed to be fully axial, thus having null tangential absolute velocity.

Both pumps require the mass flow rate as input. For the fuel, the mass flow rate is set by the mass flow rates required by the main combustion chamber and the gas-generator. The total mass flow rate through the pump is then:

$$\dot{m}_{fp} = \dot{m}_{ccf} + \dot{m}_{ggf} \tag{26}$$

here $\dot{m}_{fp}$, $\dot{m}_{ccf}$, $\dot{m}_{ggf}$ are respectively total mass flow rate through the pump, mass flow rate to the combustion chamber, and mass flow rate to the gas generator. On the other hand, for the oxygen fluid line, the total mass flow rate is set by the equation:

$$\dot{m}_{op} = N_{rad} \cdot \eta_{vol} \cdot Vol \cdot \rho \tag{27}$$

where η_{vol}, Vol, ρ are the volumetric effciency, pump volume displaced in one full rotation, and pump inlet density. In particular:

$$\eta_{pump} = \eta_{vol} \cdot \eta_{mech} \tag{28}$$

where η_{pump}, η_{mech} are the pump total efficiency and pump mechanical efficiency.

Since the mass flow rate to the gas generator is set by the LOX injector, then the mass flow rate to the combustion chamber is found with the following equation to ensure that the mass is conserved.

$$\dot{m}_{cco} = \dot{m}_{op} - \dot{m}_{ggo} \tag{29}$$

2. Turbine Governing Equations

The turbine is responsible for generating power for the two pumps, by expanding the combustion products from the gas generator. The gas generator is modeled similarly to a combustion chamber, with more details provided in Section 6. The turbine power generated is found with the following equation, assuming that the hot gas behaves as an ideal gas:

$$\dot{W}_t = \dot{m}_{gg} \cdot \eta_t \cdot Cp_{t_{in}} T_{t_{in}} \left[1 - \left(\frac{P_{in}}{P_{out}} \right)^{\frac{\gamma-1}{\gamma}} \right] \tag{30}$$

3. Shaft Governing Equations

The angular acceleration of the shaft is governed by the following ordinary differential equation:

$$\frac{dN_{rad}}{dt} = \frac{\sum T_{rq}}{\sum J} \tag{31}$$

where $Nrad, Trq, J$ are shaft speed, and moment of inertia. In particular:

$$\sum T_{rq} = T_{rq_t} - T_{rq_{op}} - T_{rq_{fp}} \tag{32}$$

$$\sum J = J_t + J_{op} + J_{fp} \tag{33}$$

C. Thrust Chamber Model

The thrust chamber is composed of the combustion chamber, which is modeled as a cylinder with a certain length and radius, and the nozzle. In this study, there are 24 combustion chambers/nozzles modules and an external plug.

1. Chamber Pressure Equations

The pressure of the gases in the combustion chamber and gas generator is modeled with the following differential equation, which can be derived starting from the conservation of mass assuming that the gas behaves like an ideal gas, and the gas flow at the nozzle throat is sonic.

$$\frac{dP_{cc}}{dt} = -\frac{P_{cc} \cdot A_{th}}{Vol_{cc}} \cdot \frac{\sqrt{\gamma \cdot \frac{R}{MW} \cdot T_{cc} \cdot \left(\frac{2}{\gamma+1}\right)^{\frac{\gamma+1}{\gamma-1}}}}{c^*_{eff}} + \frac{R \cdot T_{cc}}{MW \cdot Vol_{cc}} \cdot \left(\dot{m}_{ccf} + \dot{m}_{cco}\right) \tag{34}$$

For the gas generator $\dot{m}_{ccf}$ and $\dot{m}_{cco}$ are replaced with $\dot{m}_{ggf}$ and $\dot{m}_{ggo}$, respectively.

2. Nozzle Equations

The gas properties in the nozzle are calculated using Chemical Equilibrium and Applications (CEA), depending on the combustion chamber pressure set by Equation (34), oxidizer to mixture ratio set by the injectors, and cross section area defined by the nozzle geometry. Chemical equilibrium and isentropic expansions are assumed.
For the thrust calculation, the jet that expands on the plug plays an important role, and for this part frozen equilibrium is assumed and the thrust is calculate as:
$$F = \dot{m} \cdot v_e + A_e (P_e - P_{amb}) \tag{35}$$
For the Aerospike engine, as stated above, perfect expansion is assumed, that $P_e = P_{amb}$.

3. Injectors Equations

The injectors set the mass flow rates in the fluid lines, and they are modeled using the orifice equation:
$$\dot{m} = K(t) \cdot \sqrt{2 \cdot \rho \cdot (P_{in} - P_{out})} \tag{37}$$
In Equation 37, $K(t)$ is regulated to set the mass flow rates in the gas generator and combustion chamber for fuel and oxidizer.

The oxygen gas generator injector is here also called Thrust Control Valve (TCV), since it regulates the flow of oxygen to the gas generator in order to increase or decrease the power of the turbine. The fuel gas generator injector in this study is called Gas Generator Mixture Ratio Control Valve (GGMRCV), and it adjust the fuel mass flow rate to the gas generator to maintain the design mixture ratio, see Equation (38), based on the oxygen mass flow rate which is set by the TCV.
$$MR = \frac{\dot{m}_f}{\dot{m}_o} \tag{38}$$
The fuel combustion chamber injector in this study is called Mixture Ratio Control Valve (MRCV), and similarly to the GGMRCV, it adjusts the fuel mass flow rate to the combustion chamber to maintain the design mixture ratio, based on the oxygen mass flow rate which is set by the oxygen pump.

For the TCV, GGMRCV, and MRCV, Equation (37) is used to calculate the mass flow rate by employing PI and P controllers. These controllers adjust the flow coefficient K in Equation (37) to achieve the target mass flow rate. For the oxidizer injector in the combustion chamber, the mass flow rate ($\dot{m}_{cco}$) is already determined using Equation (29). Since the upstream and downstream pressures (P_{in} and P_{out}) in Equation 37 are known, Equation 37 is used to calculate the required K without using a controller.

Legend: P = Proportional; I = Integrator

Figure 3. Control logic of TMS

Figure 3 illustrates the functioning of the PI and P controllers used in this study. Two P controllers are employed to control the coefficient K of the GGRCV and MRCV. Additionally, a PI controller is used to adjust the coefficient K of the TCV.

D. Abnormal Scenarios and Damageability

Rocket engines can suffer from many types of damage[18]. The solid wall in the regenerative cooling system can suffer from low cycle fatigue failures due to thermal cycles caused by repeated launches. Cooling channels, valves, pipeline, and injectors can suffer from leakage and blockage, due to excess powder from printing, printing tolerances, thermal expansion, etc., reducing the mass flow rate. Pumps and turbines have many failure modes due to material degradation or abnormal operating conditions. In particular, pumps can suffer from cavitation, that can affect the efficiency, increase vibrations, and eventually damage the pump blades.

This paper investigates two types of damage: fuel injector blockage and reduced pump efficiency, assessing their effects on the cooling system.

1. Injector Blockage

Blockage can occur due to different factors, such as impurities in the propellants, or residual powder for printing, resulting in reduced mass flow rate. In this study, a reduction in the mass flow rate of methane to the combustion chamber was modeled using a gain block going from 100% to 90% of area opening. Where 100% is fully open during nominal operations, and 90% is the partially blocked case.

$$A(t) = \begin{cases} 1, & t < t_0 \\ 1 - 0.05 \cdot t, & t_0 < t < t_0 + \delta \\ 0.9, & t > t_0 + \delta \end{cases} \tag{39}$$

This damage was introduced at $t_0 = 63\ s$ from the start of the simulation, and $\delta = 2s$.

2. Pump Reduced Efficiency

Another common phenomenon in rocket pumps operating with cryogenic propellants is cavitation, which involves the formation of small bubbles in the liquid propellant if the pump inlet pressure is below the required NPSH[11]. This effect was modelled as a decrease in the pump's reduced volumetric efficiency from 90% to 85%. Consequently, with a pump mechanical efficiency of 89%, the total efficiency is also reduced.:

$$\eta_p = \eta_{vol} \cdot \eta_{mech} \tag{40}$$

In this study, this type of damage was introduced to the oxygen pump at $t = 60$ seconds from the start of the simulation. In the same simulated mission, this damage was followed by an injector blockage, which was introduced at $t = 63$ seconds.

3. Low Cycle Fatigue

Low cycle fatigue is a common failure mode for rocket engine cooling systems, involving the development of cracks in the solid wall that separates hot gas from the coolant, eventually leading to catastrophic failure[11]. Failures such as the doghouse effect are related to thermal cycles and are aggravated by the high thermal loads experienced by the solid wall of the regenerative cooling system during each flight. In this study, the decrease in the number of engine reuses due to low cycle fatigue is used as an indicator of thermal management system damage, demonstrating how damaged components can reduce the number of possible engine reuses.

There are many correlations to predict the number of thermal cycles before failure due to low cycle fatigue[19]. These correlations depend on the material, and the geometry of the structure. Smallwood[20] found the coefficients for the Smith-Watson-Topper correlation by curve fitting experimental data of the material GRCop-42, applying his finding to Rotating Detonation Rocket Engines (RDRE). Given the similarities between the aerospike engine's cooling channels geometry and that of the RDRE, as well as the shared use of GRCop-42, this study employs the coefficients found by Smallwood to assess the number of reuses due to low cycle fatigue for the aerospike engine's thermal management system.

IV. Results

The results were derived using the model outlined in the previous sections to simulate a typical mission profile. Details about the mission profile are provided below.

A. Mission Profile

The mission profile is inspired by the space shuttle ascent phase[21] but can also be found in other works on current rocket launchers[22]. The aerospike engine used in this study is assumed to be the engine for the booster stage, meaning it will travel from the launchpad to orbit. Therefore, the ascent mission profile is the same as that described for the Space Shuttle[21], and it is illustrated in Figure 4.

The thrust profile required for the hypothesized mission involves an initial phase at 100% thrust, followed by a phase where the engine throttles down to 85% for 5 seconds when the

Figure 4. Thrust level during mission.

rocket experiences the maximum dynamic pressure (max q). The engine then returns to 100% thrust until orbit is reached at $t = 110$ seconds.
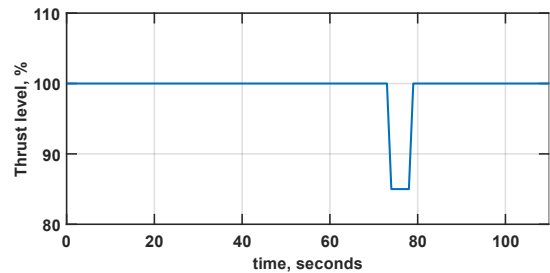
B. Nominal Case

The model discussed above was used to conduct simulations in two different scenarios. The first scenario follows the nominal mission profile outlined in Section E. Figures 5-7 present the results for various components during this simulation.

To size TMS components such as pumps, gas generators, combustion chambers, nozzles, and injectors, confidential steady-state reference data for key engine parameters were used. These parameters include pump discharge pressure, thrust, combustion chamber pressure, and the mass flow rates of fuel and oxidizer in both the combustion chamber and gas generator. These confidential values served as the normalization basis for pump outlet pressure, combustion chamber pressure, and fuel and oxidizer mass flow rates shown in Figures 5-7. The model yielded normalized values close to 1 under nominal conditions, demonstrating that it accurately predicts the expected performance of each component.

Moreover, even for quantities lacking direct reference data, the simulation produced physically consistent trends that depend on the validated parameters. These values were also normalized by their steady-state values obtained from the simulation. This approach further confirms that the model accurately predicts the expected performance of each component under nominal conditions while ensuring overall reliability.

a)   Normalized engine thrust.

b)   Normalized shaft speed.

c)   Normalized turbine power.

d)   Normalized LOX pump power.

e)   Normalized LOX pump outlet pressure.

f)   Normalized combustion chamber pressure.
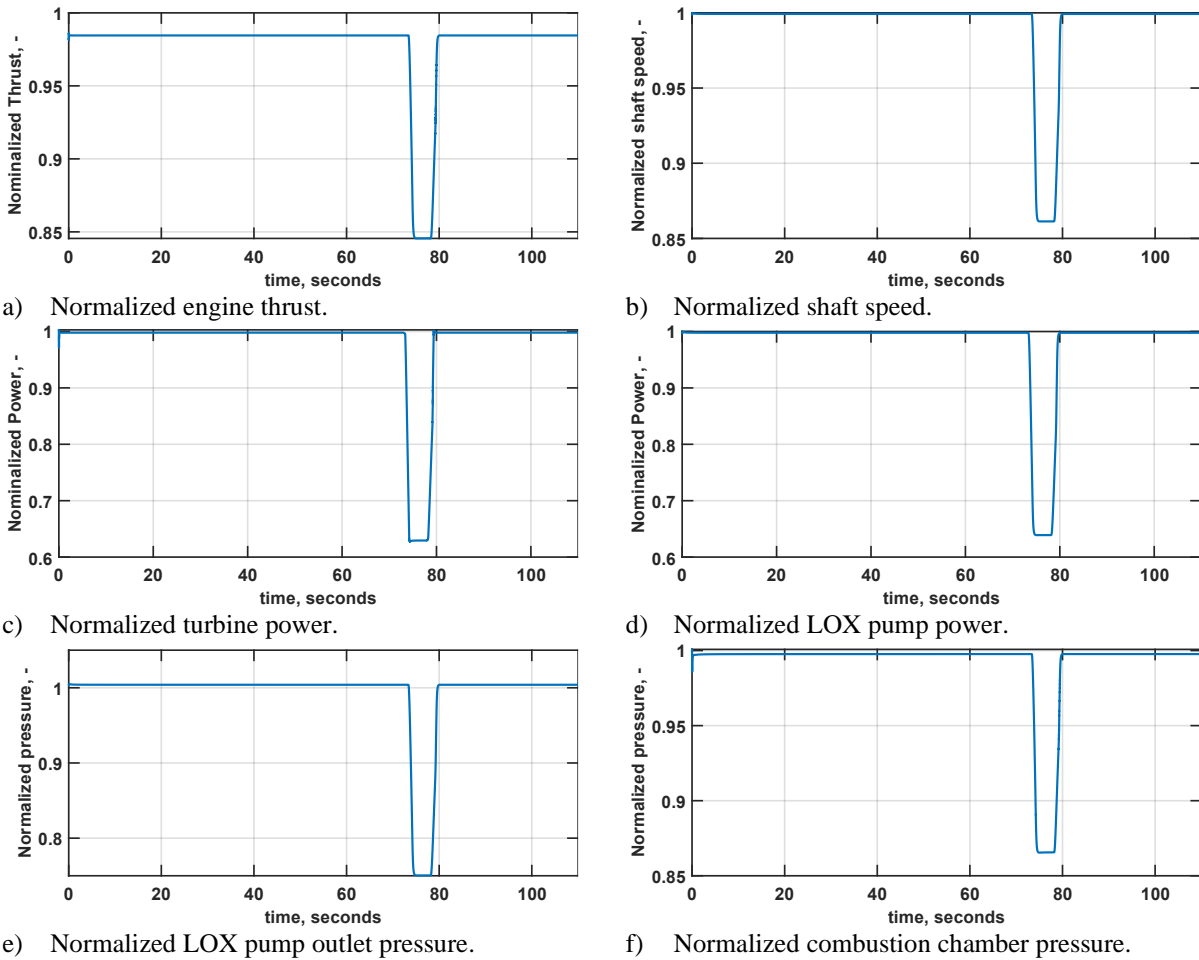
Figure 5. Numerical results under nominal conditions of engine thrust and chamber pressure, and turbopumps power and pressure.
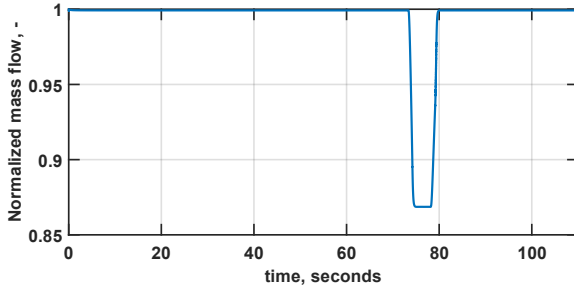
International Conference on Environmental Systems

a) Normalized LOX mass flow rate in the combustion chamber.
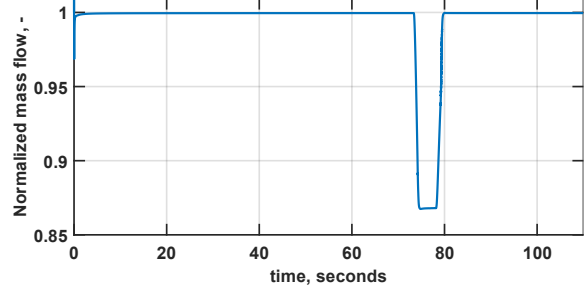
b) Normalized methane mass flow rate in the combustion chamber.
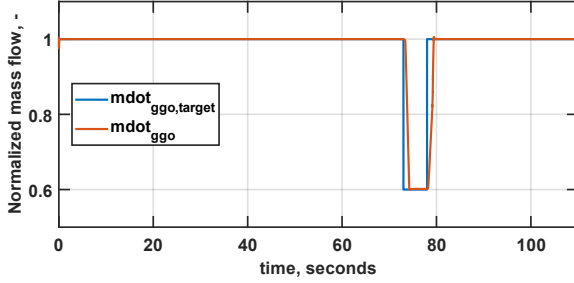
c) Normalized LOX mass flow in the gas generator.
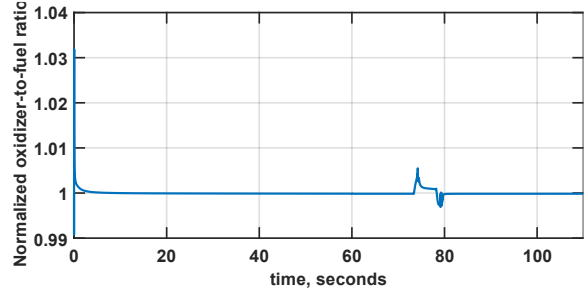
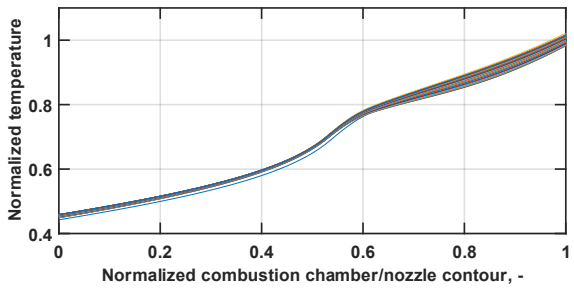d) Normalized oxidizer-to-fuel ratio in the combustion chamber

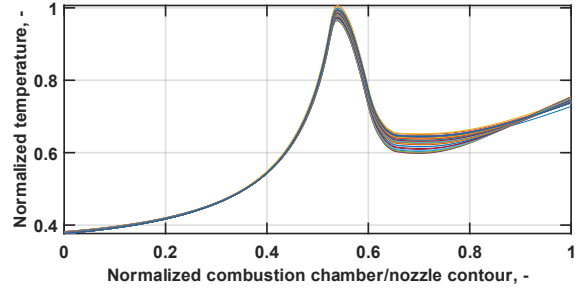**Figure 6. Numerical results under nominal conditions of mass flow rates.**
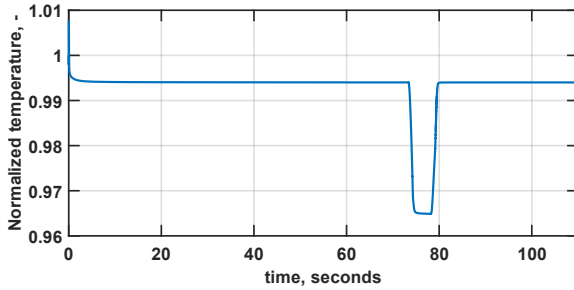
a) Normalized maximum gas-side wall temperature.
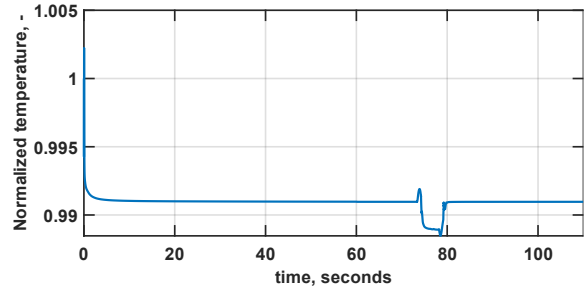
b) Normalized maximum cool-side wall temperature.

c) Normalized LOX temperature distribution in time and along nozzles/combustion chambers.

d) Normalized gas-side wall temperature along nozzles/combustion chambers.

Figure 7. Numerical results under nominal conditions of temperature in the cooling system.

As shown in Figure 5(a), the thrust profile ranges from 98% to 85% during the max q phase of the flight, illustrating the reduction in thrust during this throttling period. The thrust calculated by the model using Equation 35 was 2% less than the nominal steady-state value (100% thrust), indicating the model's acceptable accuracy in returning an accurate value.

Figure 5(b) shows that the shaft speed is reduced due to the lower power required and generated by the system during the throttling phase at lower thrust. Additionally, it is worth noting that once the model throttles back up to full thrust after max q, it returns to steady-state behavior, settling again at the values observed before the max q maneuver.

Figure 6(d) demonstrates that the O/F ratio is maintained almost constant during the simulation by the PI and P controllers in the MRCV and GGMRCV, even as the mass flow rates of fuel and oxidizer change due to throttling (Figure 6(a-b)). Regarding the cooling jackets, Figure 7(a-b) show that the maximum wall temperature on both sides reaches a steady state before, during, and after max q, confirming that the model adapts each component to different mission phases.

During the throttling phase at 85% thrust, there is a lower mass flow rate for both generating thrust and cooling the engine, as seen in Figure 6(a). However, while this could lead to a higher wall temperature due to a lower coolant heat transfer coefficient, Figure 7(a-b) shows that the wall temperature is not affected by this decrease in mass flow rate. This is because the lower mass flow rate in the combustion chamber reduces the chamber pressure (Figure 5(f)) and temperature, thereby lowering the gas heat transfer coefficient and reducing heat transfer to the combustion chamber/nozzle wall.

Figure 7(c-d) illustrates the temporal evolution of the coolant and wall temperature profile along the combustion chamber/nozzle contour. For example, in Figure 7(d), the wall temperature profile stabilizes at a steady-state value during the full thrust phase and then decreases to the minimum wall temperature profile during the 85% thrust phase.

Figures 5-7 show an initial oscillation in the numerical results for the first 5 seconds of the simulated time. This occurs because the PI and P controllers require initial data from the simulation before they can converge to their setpoints.

C. Damaged Case

In this second case, two types of damage were introduced to the aerospike engine system, and their effects on the regenerative cooling system were investigated. The results can be seen in Figures 8-11 below. As with the previous case, these results have been normalized using the same values as those used for the numerical results in Figures 5-7.
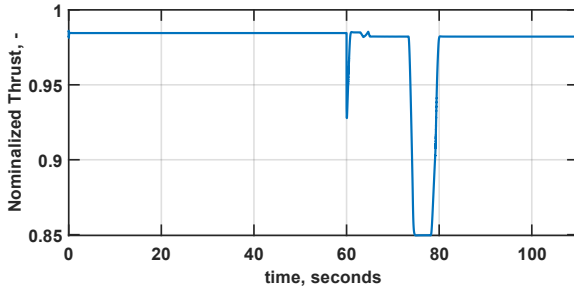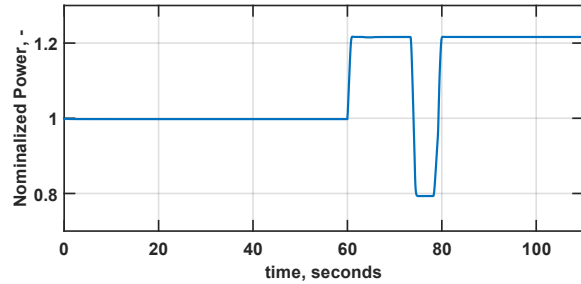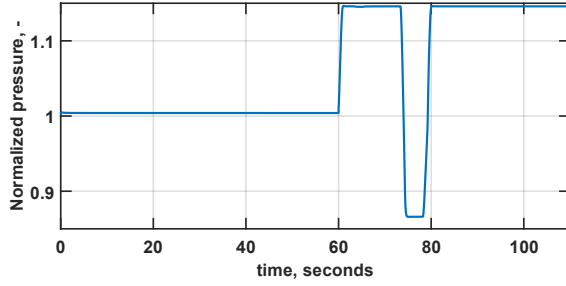

a)   Normalized engine thrust.
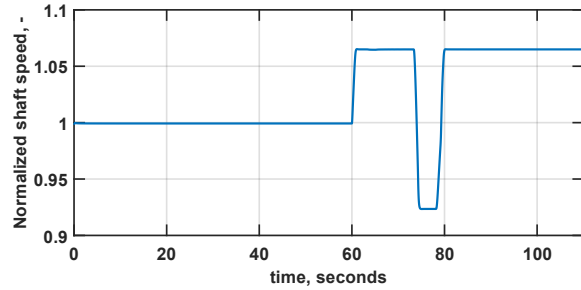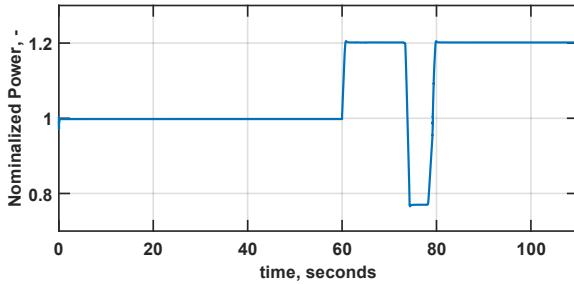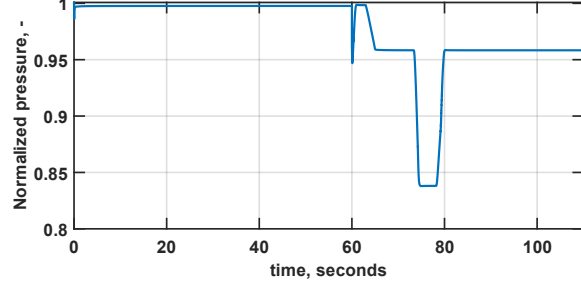
b)   Normalized shaft speed.

c)   Normalized turbine power.
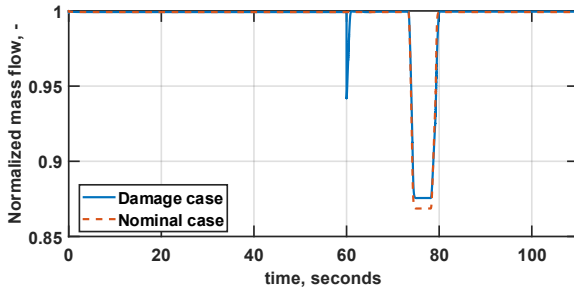
d)   Normalized LOX pump power.
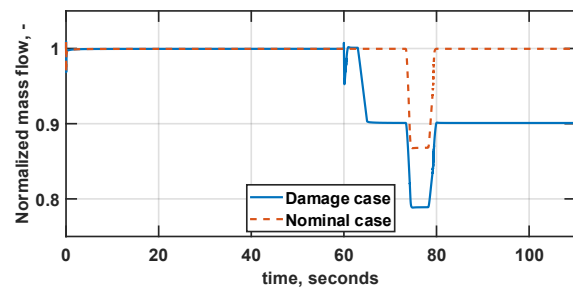
e) Normalized LOX pump outlet pressure.

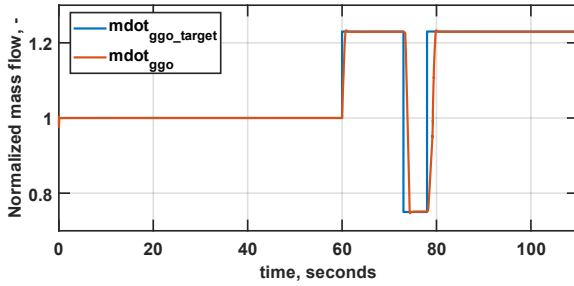f) Normalized combustion chamber pressure.

Figure 8. Numerical results under damaged conditions of engine thrust and chamber pressure, and turbopumps power and pressure.
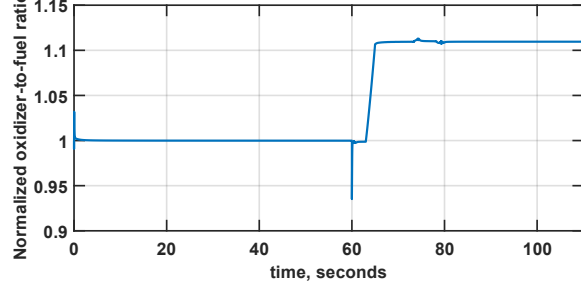

a) Normalized LOX mass flow rate in the combustion chamber.

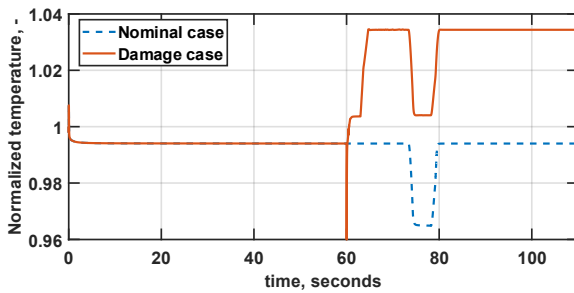b) Normalized methane mass flow rate in the combustion chamber.

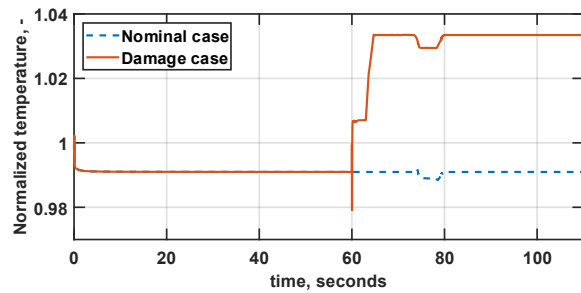c) Normalized LOX mass flow in the gas generator.

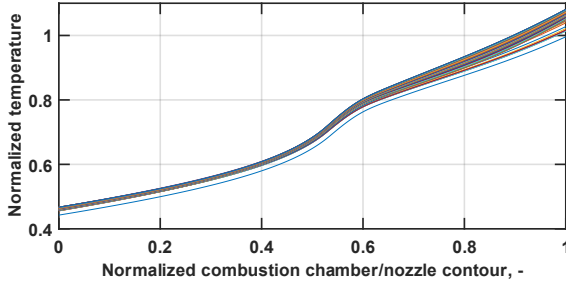d) Normalized oxidizer-to-fuel ratio in the combustion chamber.

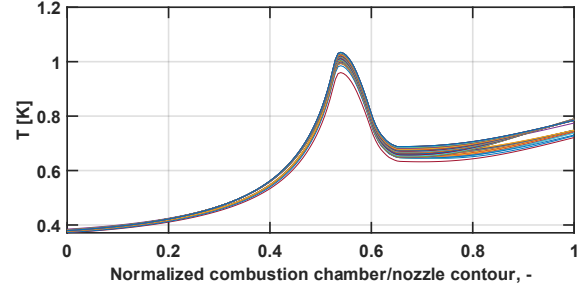**Figure 9. Numerical results under damaged conditions of mass flow rates.**

a) Normalized maximum gas-side wall temperature.

b) Normalized maximum cool-side wall temperature.

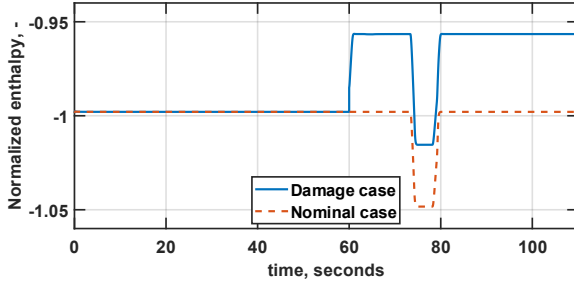International Conference on Environmental Systems

c) Normalized LOX temperature distribution in time
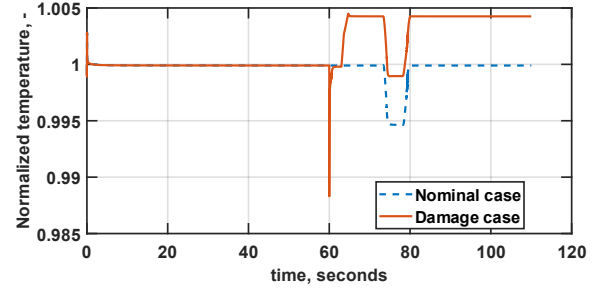   and along nozzles/combustion chambers.

d) Normalized gas-side wall temperature along
    nozzles/combustion chambers.

Figure 10. Numerical results under damaged conditions of temperature in the cooling system.

a) Normalized enthalpy of oxygen at pump outlet.

b) Normalized maximum gas temperature.

Figure 11. Numerical results under damaged conditions of LOX pump enthalpy and gas temperature.

Figure 8(d) shows the pump outlet pressure before and after the reduction in efficiency. At $t = 60$ seconds, the volumetric efficiency of the pump decreases from 90% to 85%, and the total efficiency drops from 80% to 75.6% due to this reduced η_{vol} .

As the pump efficiency lowers, the mass flow rate supplied by the pump reduces, as shown in Figure 9(a) at $t = 60$ seconds. Additionally, lower efficiency will cause the pump to absorb more power, requiring the turbine to generate more power to compensate for the increased power consumption of the oxidizer pump and maintain the desired thrust level (Figure 8(c-d)). To achieve this, the gas generator needs a higher mass flow rate. Figure 9(c) shows that the Thrust Control Valve (TCV) directs more oxygen propellant to the gas generator to increase turbine power, making its working conditions substantially different from the design values. This increases the power generated by the turbine, raises the shaft speed (Figure 8(b)), and consequently increases the mass flow rate supplied by the pump until $\dot{m}_{cco}$ returns to the pre-damage mass flow rate. However, this comes at the cost of higher shaft speed and increased mass consumption in the gas generator, which does not contribute to thrust. As a result, the enthalpy at the pump outlet increases (Figure 11(a)), raising the inlet temperature of the cooling channels. This reduces the heat flux to the coolant, thereby increasing the wall temperature. Figure 10(a) illustrates the time evolution of the maximum gas-side wall temperature, with its distribution along the nozzle contour depicted in Figure 10(d). Figure 10(a-b) shows the initial temperature rise on both sides of the wall immediately following the pump damage.

Another damage was also introduced at $t = 63$ seconds: a fuel injector blockage in the combustion chamber, which reduces the fuel mass flow rate to the combustion chamber, and the methane-cooled heat exchanger as well, as shown in Figure 9(b).

The primary effect of the methane injector blockage is a change in the oxidizer-to-fuel ratio. As shown in Figure 9(d), the O/F ratio increases, leading to higher temperatures in the combustion chamber (Figure 11(b)) and, consequently, increased heat flux to the combustion chamber walls. This results in an additional rise in gas-side wall temperature at 63 seconds, as depicted in Figure 10(a-b), following the initial temperature increase caused by the pump damage at 60 seconds.

V.   Discussion

Figure 12 illustrates the reduction in the number of available engine restarts, demonstrating that operating the engine at higher temperatures decreases the number of reuses before a Low Cycle Fatigue (LCF) failure occurs. In Figure 12, the number of available restarts is normalized by the number of restarts at the lower temperature value, while the temperature is normalized by the maximum value along the nozzle contour. Smallwood[20] uses three different sets of coefficients within the Ramberg-Osgood formulation to estimate the stress range from the plastic strain range. Nominal coefficients, derived from curve fitting to GRCop-42 experimental data, predict most of the observed stress-strain behavior. Upper and lower bounds are defined by adding and subtracting multiples of the standard deviation from the mean curve, using 9 for the upper bound and 3 for the lower bound, to account for data uncertainty.

These coefficients are then used in the Ramberg-Osgood equation and the Smith Watson Topper model to predict the available number of engine reuses at different operating temperatures, as illustrated in Figure 12. In particular, the number of reuses decreases due to the increased maximum wall temperature caused by pump and injector damage. More details about these calculations can be found in Section 11 and Reference (20). As shown in Figure 10(a-b), the maximum wall temperature during the damaged scenario increases on both the gas-side and cool-side, exceeding the temperatures observed under nominal conditions. These elevated temperatures accelerate material low cycle fatigue, as illustrated in Figure 12, leading to a 16% reduction in the predicted number of reuses for the upper bound case, and a 15% reduction for both the nominal and lower bound cases.
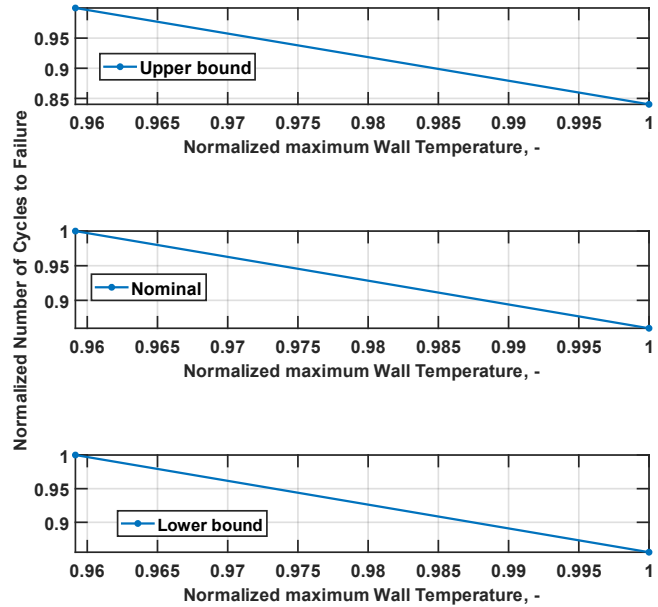

Figure 12. Number of cycles to low cycle fatigue

VI.   Conclusion

The numerical model introduced in this study generates data to support the future resilient design of aerospike engines' thermal management systems (TMS). To achieve reliable data for the aerospike TMS, the model is based on the physics equations of each major component.

To demonstrate the TMS model, two types of numerical results are provided. The first set of results shows the behavior of the TMS under nominal conditions during a typical ascent mission. The second set demonstrates that the TMS numerical model can also predict TMS behavior during abnormal scenarios, such as pump damage and fuel injector blockage.

This study also shows that damage to the thermal management system affects the lifespan of the cooling system's solid wall. The reduced lifespan, quantified by the number of available reuses, was plotted against operating temperature experienced by the heat exchanger wall made of GRCop-42.

Future work includes developing a resilient aerospike TMS design through system reconfiguration, corrective actions, and control strategies. Additionally, integrating improved heat transfer coefficient correlations and validating with transient experimental data will enhance model fidelity and, consequently, system resilience.

Acknowledgments

References

[1]Hagemann, G., Immich, H., Nguyen, T. V., and Dumnov, G. E., "Advanced Rocket Nozzles," *Journal of Propulsion and Power*, Vol. 14, No. 5, 1998.

[2]Russo Sorge, A., Carmicino, C., and Nocito, A., "Design of a Lab-Scale Cooled Two-Dimensional Plug Nozzle for Experimental Tests," *Proceedings of the 38th AIAA/ASME/SAE/ASEE Joint Propulsion Conference & Exhibit*, AIAA Paper 2002-4039, Indianapolis, IN, July 2002.

[3]Vuillamy, D., Duthoit, V., and Berry, W., "European Investigation of Clustered Plug Nozzles," *Proceedings of the 35th AIAA/ASME/SAE/ASEE Joint Propulsion Conference & Exhibit*, AIAA Paper 99-2350, Los Angeles, CA, June 1999.

[4]Hagemann, G., Schley, C.-A., Odintsov, E., and Sobatchkine, A., "Nozzle Flowfield Analysis with Particular Regard to 3D-Plug Cluster Configurations," *Proceedings of the 32nd AIAA/ASME/SAE/ASEE Joint Propulsion Conference & Exhibit*, AIAA Paper 96-2954, Lake Buena Vista, FL, July 1996.

[5]Pizzarelli, M., Nasuti, F., and Onofri, M., "Effect of Cooling Channel Aspect Ratio on Rocket Thermal Behavior," *Journal of Thermophysics and Heat Transfer*, Vol. 28, No. 3, 2014.

[6]Mullin, W., Melendez, K., Stefanko, B., Bell, A., Davis, G., and Adu, E., "Evaluating Regenerative Cooling Channels for Nuclear Thermal Propulsion with Additive Manufacturing," *Proceedings of the AIAA SciTech 2022 Forum*, AIAA Paper 2022-2309, San Diego, CA, Jan. 2022.

[7]Jeon, T. J., and Park, T. S., "Thermal Recycling Analysis in Regenerative Cooling Channels Based on Liquid Rocket Engine Cycles," *Applied Thermal Engineering*, Vol. 256, 2024, Paper 124095.

[8]Heister, S. D., Anderson, W. E., Pourpoint, T., and Cassady, R. J., *Rocket Propulsion*, Cambridge University Press, Cambridge, U.K., 2019, p 177-197.

[9]Behbahani, A. R., Macmann, O., Seitz, T., and Buettner, R., "Framework for Integrated Robust and Resilient Control of Propulsion Systems for Reliability and Performance," *Proceedings of the 52nd AIAA/SAE/ASEE Joint Propulsion Conference*, AIAA Paper 2016-4869, Salt Lake City, UT, July 2016.

[10]Rossi, F., Esnault, G., Sápi, Z., Palumbo, N., Argemí, A., and Bergström, R., "Research Activities in the Development of DEMOP1: A LOX/LNG Aerospike Engine Demonstrator," *7th Edition of the Space Propulsion Conference*, Estoril, Portugal, March 2021.

[11]Sutton, G. P., and Biblarz, O., *Rocket Propulsion Elements*, 9th ed., Wiley, Hoboken, NJ, 2016, pp 310-313, 365-387.

[12]Gradl, P. R., Protz, C., Cooper, K., Garcia, C., Ellis, D., and Evans, L., "GRCop-42 Development and Hot-Fire Testing Using Additive Manufacturing Powder Bed Fusion for Channel-Cooled Combustion Chambers," *Proceedings of the 55th AIAA/SAE/ASEE Joint Propulsion Conference*, AIAA Paper 2019-4228, Indianapolis, IN, July 2019.

[13]Marucho, M. D., and Campo, A., "Suitability of the Method of Lines for Rendering Analytic/Numeric Solutions of the Unsteady Heat Conduction Equation in a Large Plane Wall with Asymmetric Convective Boundary Conditions," *International Journal of Heat and Mass Transfer*, Vol. 99, 2016, pp. 201–208.

[14]Pizzarelli, M., Nasuti, F., Onofri, M., Roncioni, P., Votta, R., and Battista, F., "Heat Transfer Modeling for Supercritical Methane Flowing in Rocket Engine Cooling Channels," *Applied Thermal Engineering*, Vol. 75, 2015, pp. 600–607.

[15]Bartz, D. R., "A Simple Equation for Rapid Estimation of Rocket Nozzle Convective Heat Transfer Coefficients," *Journal of Jet Propulsion*, Vol. 27, No. 1, 1957, pp. 49–51.

[16]Incropera, F. P., DeWitt, D. P., Bergman, T. L., and Lavine, A. S., Fundamentals of Heat and Mass Transfer, 6th ed., John Wiley & Sons, Hoboken, NJ, 2007., pp 514-516.

[17]Miranda, A. W., and Naraghi, M. H., "Analysis of Film Cooling and Heat Transfer in Rocket Thrust Chamber and Nozzle," *Proceedings of the 49th AIAA Aerospace Sciences Meeting including the New Horizons Forum and Aerospace Exposition*, AIAA Paper 2011-712, Orlando, FL, Jan. 2011.DOI: 10.2514/6.2011-712.

[18]Zhang, W., *Failure Characteristics Analysis and Fault Diagnosis for Liquid Rocket Engines*, National Defense Industry Press & Springer.

[19]Iyer, D. S., and Pillai, N. C., "Advanced Models for Fatigue Life Estimation of Combustor Components for Gas Turbine Application," *Proceedings of the ASME 2019 Gas Turbine India Conference (GTINDIA2019)*, Paper GTINDIA2019-2380, Chennai, India, Dec. 2019.

[20]Smallwood, J., Heister, S., and Sangid, M. D., "Structural Life Characterization of a Rotating Detonation Rocket Engine (RDRE)," Proceedings of the AIAA SciTech 2025 Forum, AIAA Paper 2025-1977, Orlando, FL, Jan. 2025.

[21]Van Hooser, K. P., and Bradley, D. P., "Space Shuttle Main Engine—The Relentless Pursuit of Improvement".

[22]Bykerk, T., Karl, S., Laureti, M., Ertl, M., and Ecker, T., "Retro-Propulsion in Rocket Systems: Recent Advancements and Challenges for the Prediction of Aerodynamic Characteristics and Thermal Loads," *Progress in Aerospace Sciences*, Vol. 151, 2024, Article 101044.

[23]Pangea Aerospace website, https://pangeaaerospace.com/ .